JPET Fast Forward. Published on February 4, 2021 as DOI: 10.1124/jpet.120.000371
This article has not been copyedited and formatted. The final version may differ from this version.

Title: Understanding exposure-receptor occupancy relationships for metabotropic glutamate receptor 5 ($mGlu_5$) negative allosteric modulators across a range of pre-clinical and clinical studies

Authors: Kirstie A Bennett, Eugenia Sergeev, Cliona P MacSweeney, Geor Bakker, Anne E Cooper

KAB, ES, CPM, GB, AEC: Sosei Heptares, Cambridge, United Kingdom

JPET Fast Forward. Published on February 4, 2021 as DOI: 10.1124/jpet.120.000371
This article has not been copyedited and formatted. The final version may differ from this version.

Running Title: Exposure-receptor occupancy relationships for $mGlu_5$ NAMs

Corresponding Author: Dr Eugenia Sergeev, Sosei Heptares, Steinmetz Building, Granta Park, Great Abington, Cambridgeshire, CB21 6DG, UK.

Email: eugenia.sergeev@soseiheptares.com Telephone: +44 (0) 1223 949 140

Number of text pages 43

Number of tables 5

Number of figures 2

Number of references 56

Number of words in

Abstract 249

Introduction 770

Discussion 1790

Non-standard abbreviations:

CSF: Cerebro-spinal fluid

fu: Free fraction

Kp: Brain/plasma ratio

Kpuu: Unbound brain/unbound plasma

$mGlu_5$: Metabotropic glutamate 5 receptor

NAM: Negative allosteric modulator

PD-LID: Levodopa-induced dyskinesia in Parkinson's Disease

RO: Receptor occupancy

Recommended Section Assignment: Drug Discovery and Translational Medicine

JPET Fast Forward. Published on February 4, 2021 as DOI: 10.1124/jpet.120.000371
This article has not been copyedited and formatted. The final version may differ from this version.

Abstract

The metabotropic glutamate receptor 5 ($mGlu_5$) is a recognized CNS therapeutic target for which several negative allosteric modulators (NAM) drug candidates have or are continuing to be investigated for various disease indications in clinical development. Direct measurement of target receptor occupancy (RO) is extremely useful to help design and interpret efficacy and safety in nonclinical and clinical studies. In the $mGlu_5$ field, this has been successfully achieved by monitoring displacement of radiolabeled ligands, specifically binding to the $mGlu_5$ receptor, in the presence of an $mGlu_5$ NAM using *in vivo* and *ex vivo* binding in rodents and positron emission tomography imaging in cynomolgus monkey and humans. The aim of this study was to measure the RO of the $mGlu_5$ NAM, HTL0014242, in rodents and cynomolgus monkey and to compare its plasma, and brain, exposure-RO relationships with those of clinically tested $mGlu_5$ NAMs dipraglurant, mavoglurant and basimglurant. Potential sources of variability that may contribute to these relationships were explored. Distinct plasma exposure-response relationships were found for each $mGlu_5$ NAM with >100-fold difference in plasma exposure for a given level of RO. However, a unified exposure-response relationship was observed when both unbound brain concentration and $mGlu_5$ affinity were considered. This relationship showed <10-fold overall difference, fitted with a Hill slope which was not significantly different from 1 and appeared consistent with a simple E_{max} model. This is the first time this type of comparison has been conducted, demonstrating a unified brain exposure-RO relationship across several species and $mGlu_5$ NAMs with diverse properties.

JPET Fast Forward. Published on February 4, 2021 as DOI: 10.1124/jpet.120.000371
This article has not been copyedited and formatted. The final version may differ from this version.

Significance Statement

Despite the long history of $mGlu_5$ as a therapeutic target and progression of multiple compounds to the clinic, no formal comparison of exposure-receptor occupancy relationships has been conducted. Our data indicate for the first time that a consistent, unified relationship can be observed between exposure and $mGlu_5$ receptor occupancy when unbound brain concentration and receptor affinity are taken into account across a range of species for a diverse set of $mGlu_5$ NAMs, including a new drug candidate, HTL0014242.

JPET Fast Forward. Published on February 4, 2021 as DOI: 10.1124/jpet.120.000371
This article has not been copyedited and formatted. The final version may differ from this version.

Introduction

Glutamate is a major excitatory neurotransmitter playing an important role throughout the nervous system via activation of metabotropic (G protein-coupled) and ionotropic (ion channel) glutamate receptors including the metabotropic glutamate 5 ($mGlu_5$) receptor. $mGlu_5$ receptors are widely distributed in the brain including the cortex, striatum, hippocampus, and cerebellum (Patel et al., 2007), mainly concentrated in post-synaptic structures and, with a few exceptions, almost undetectable in pre-synaptic structures (Hovelsø et al., 2012; Ferraguti and Shigemoto, 2006; Berthele et al., 1999). In diseases where glutamatergic signalling is dysregulated (e.g. depression, anxiety, addiction, neuropathic pain and levodopa-induced dyskinesia; Archer and Garcia, 2016; Emmitte, 2013; Slassi et al., 2005), enhanced $mGlu_5$ receptor activation can lead to increased transsynaptic glutamate release which could further exacerbate glutamate-mediated excitotoxic processes. Antagonists, or negative allosteric modulators (NAMs), of the $mGlu_5$ receptor have therapeutic potential in a range of psychiatric and neurological disorders characterised by glutamatergic hyperexcitability (Gregory et al., 2011[a]). NAMs block the effects of glutamate by binding in the seven transmembrane bundle of the receptor, rather than at the orthosteric glutamate binding site in the Venus Flytrap Domain (Pagano et al., 2000; Christopher et al., 2015). NAMs have avoided the problems associated with targeting the orthosteric site including lack of selectivity, poor pharmacokinetics and low CNS penetration (Lindsley and Stauffer, 2013).

Several $mGlu_5$ NAMs have progressed to clinical trials. Dipraglurant and mavoglurant showed promising results in reducing levodopa-induced dyskinesia in Parkinson's Disease (PD-LID) in Phase II trials (Tison et al., 2016; Stocchi et al., 2013), although mavoglurant failed to demonstrate efficacy in subsequent Phase IIb studies (Trenkwalder et al., 2016). When administered as an adjunctive therapy in major depression (Phase IIb), basimglurant

JPET Fast Forward. Published on February 4, 2021 as DOI: 10.1124/jpet.120.000371
This article has not been copyedited and formatted. The final version may differ from this version.

failed to demonstrate efficacy on primary endpoints although there were significant effects on secondary endpoints (e.g. Montgomery-Åsberg Depression Rating Scale; Quiroz et al., 2016). Clinical trials are in progress to further evaluate therapeutic opportunities, including PD-LID (dipraglurant) and substance-use disorders (mavoglurant). It is worth noting that several $mGlu_5$ NAMs have reported dose-related adverse events in clinical trials (Kågedal et al., 2013, Kalliomake et al., 2013 Trenkwalder et al., 2016, Jaso et al., 2017, NCT01348087), and it is currently unclear whether it was possible to achieve sufficient $mGlu_5$ NAM exposure to fully explore efficacious potential.

Measurement of receptor occupancy (RO) is useful in designing efficacy and safety studies to ensure that the therapeutic concept is tested and/or to aid interpretation of any adverse events. There have been numerous publications on specific pharmacokinetic exposures and/or measured $mGlu_5$ RO for $mGlu_5$ NAMs across species (Anderson et al., 2002, Hamill et al., 2005, Kågedal et al., 2013, Gregory et al., 2014[b], Lindermann et al., 2015, Xu and Li, 2019). Different approaches to the determination of RO have been used, including direct binding following exposure *in vivo* or *ex vivo* to radioligands (Able et al., 2011) or indirectly by measuring radioligand displacement. Preclinically, $mGlu_5$ radioligands [^{3}H]methoxy-MPEP ([^{3}H]M-MPEP; Gasparini et al., 2002) and [^{3}H]methoxy-MTEP ([^{3}H]M-MTEP; Anderson et al., 2002) have been used extensively. Positron emission tomography (PET) can be used in both preclinical and clinical settings and several $mGlu_5$ PET ligands have been developed, allowing quantitative measurement of receptor expression and distribution across brain regions, and RO of $mGlu_5$ compounds following systemic drug administration. The most widely used are [^{11}C]ABP688 (Ametamey et al., 2007) and [^{18}F]FPEB (Sullivan et al., 2013; Wong et al., 2013[a]), which have been shown to bind to the same site as MPEP in rodent (Wyss et al., 2007; Hintermann et al., 2007) and monkey brain (Hamill et al., 2005), respectively. A different PET ligand, [^{11}C]RO511232 was developed and used clinically for

JPET Fast Forward. Published on February 4, 2021 as DOI: 10.1124/jpet.120.000371
This article has not been copyedited and formatted. The final version may differ from this version.

basimglurant (NCT 01483469), although [^{11}C]ABP688 was used preclinically (Lindermann et al., 2015).

Although there is extensive published experience with $mGlu_5$ PET ligands (Lohith et al., 2017, Wong et al., 2013[a], Kågedal et al., 2013), there is limited understanding of RO in relation to drug exposure, how it aligns across species and how exposure-response relationships compare between $mGlu_5$ NAMs. As understanding exposure-$mGlu_5$ RO relationships is important in achieving the right level of $mGlu_5$ target engagement for positive efficacy in a therapeutic setting, we studied the plasma and brain exposure-RO relationships of dipraglurant, basimglurant, mavoglurant and HTL0014242, a new $mGlu_5$-selective NAM (Christopher et al., 2015). The comparative data for this analysis is derived from experimental data and supplemented by published $mGlu_5$ RO and exposure data across species (Bennett et al., 2014, Lindermann et al., 2015, Quiroz et al., 2016, Tison et al., 2016, Cosson et al., 2018). As this study will demonstrate, when accounting for $mGlu_5$ affinity and brain exposure, exposure-RO relationships were similar across species and different $mGlu_5$ NAMs, and in agreement with the simple E_{max} model.

JPET Fast Forward. Published on February 4, 2021 as DOI: 10.1124/jpet.120.000371
This article has not been copyedited and formatted. The final version may differ from this version.

Materials and Methods

Chemicals

Mavoglurant ((3aR,4S,7aR)-4-hydroxy-4(3-methylphenyl)ethynyl-octahydro-indole-1-carboxylic acid methyl ester); dipraglurant (6-Fluoro-2-(4-[pyridin-2-yl]but-3-yn-1yl)imidazo[1,2-a]pyridine) and HTL0014242 (3-chloro-5-[6-(5-fluoropyridin-2-yl)pyrimidin-4-yl]benzonitrile) were synthesised by Sosei Heptares. Basimglurant ([2-chloro-4-[1-(4-fluoro-phenyl)-2-methyl-1H-imidazol4-ylethynyl]-pyridine) was purchased from MedChemExplorer (catalogue number HY-15446).

Radiotracers

For the mouse and rat *ex vivo* occupancy experiments, [^{3}H]M-MPEP (2-[(3-methoxyphenyl)ethynyl]-6-methylpyridine) was custom synthesized by Tritec (specific activity 67 Ci/mmol). For the mouse *in vivo* occupancy experiments, [^{3}H]M-MPEP was purchased from American Radiolabeled Chemicals, Inc (St. Louis, MO; Cat# art1571; specific activity 80 Ci/mmol).

[^{18}F]FPEB (3-[^{18}F]fluoro-5-[(pyridin-3-yl)ethynyl] benzonitrile) for the rat PET study was synthesized by Invicro, whilst for the cynomolgus monkey PET study the tracer was prepared at GE Healthcare. For the rat PET study synthesis of [^{18}F]fluoride at Invicro was done using a Siemens RDS-111 Eclipse cyclotron equipped with a fluoride target loaded with oxygen-18 enriched water by means of ^{18}O(p,n)^{18}F reaction. Optimization of yield was achieved by using a spirocyclic iodonium ylide (SCIDY) precursor (Stephenson et al., 2015). For full details see Varlow et al., 2020. For the cynomolgus monkey PET study, [^{18}F]FPEB was prepared by GE TRACERlab™ FX-FN using the following methodology. Commercially purchased [^{18}F]fluoride was transferred onto and trapped on an ion exchange cartridge.

JPET Fast Forward. Published on February 4, 2021 as DOI: 10.1124/jpet.120.000371
This article has not been copyedited and formatted. The final version may differ from this version.

Following elution with K2CO3 (1 mg) and K222 (10 mg), the [^{18}F]fluoride was dried under vacuum and helium flow under azeotropic conditions. After completion, precursor dissolved in DMSO was added (5 mg in 1.0 mL) and the reaction mixture was heated to 150°C for 10 min being before cooled and diluted with water. The solution was transferred through a solid phase extraction cartridge followed by acetonitrile elution (2 mL) into 3 mL of H_2O and HPLC injection. Product was collected with HPLC purification (Phenomenex Luna C18(2)) and acetonitrile/water (45/55, 5 mL/min) and subsequently formulated in physiological solution after solid phase extraction.

All other drugs, chemicals, cell culture reagents, and consumables were purchased from commercial sources.

Animals

Mouse *in vivo* RO studies: Male C57Bl/6 mice (25-30 g; Charles River, Rayleigh, NC) were used. All procedures were approved by the Institutional Animal Care and Use Committee in accordance with *The Guide for the Care and Use of Laboratory Animals*.

Mouse *ex vivo* occupancy and *ex vivo* K_i studies: Male CD1 mice (approximately 30 g; Charles River, Margate, Kent) were used. All experiments were performed in accordance with UK home office regulations and in line with the Animals Scientific Procedures Act (ASPA; 1986) and the transposed EU directive 2016/63/EU. Studies were conducted at Royal Veterinary College following institutional review board approval.

Rat *ex vivo* RO: Male Sprague-Dawley rats (250-300g; Charles River, Margate, Kent) were used. Rat PET imaging: Male Sprague Dawley rats (350-450 g; Charles River, Margate, Kent) were used. Both experiments were performed in accordance with UK Home Office regulation and in line with the ASPA and transposed EU directive 2016/63/EU.

JPET Fast Forward. Published on February 4, 2021 as DOI: 10.1124/jpet.120.000371
This article has not been copyedited and formatted. The final version may differ from this version.

Cynomolgus monkey PET imaging: Two adult cynomolgus monkeys (*Macaca fascicularis*), 1 female 8 years old and 1 male 16 years old. This study was conducted in full compliance with Yale University's Institutional Animal Care and Use Committee (IACUC) policies and procedures, which follow the recommendations of *The Guide for the Care and Use of Laboratory.*

K_i Determination

[^{3}H]M-MPEP saturation binding and competition binding assays were performed at human, rat, mouse and cynomolgus monkey $mGlu_5$ following the methods described in Christopher et al., 2015 either using membranes prepared from human embryonic kidney 293 cells (HEK293) transiently transfected with the receptor for human, rat and cynomolgus monkey $mGlu_5$ or membranes prepared from frontal cortices isolated from adult male CD1 mice prepared according to the method described in Robertson et al., 2011 for mouse $mGlu_5$. The radioligand employed is based on the $mGlu_5$ NAM M-MPEP and has been reported to bind to the same allosteric site as the $mGlu_5$ NAMs tested in the competition binding assay (Doré et al. 2014). Furthermore, complete inhibition of [^{3}H]M-MPEP binding to $mGlu_5$ has been reported for mavoglurant and dipraglurant (Doré et al. 2014) as well as HTL0014242 (Sergeev et al. 2018). Therefore, the Cheng-Prusoff equation could be applied to derive K_i values from the IC_{50} values that resulted from a four-parameter logistic equation fit of the competition binding data.

Mouse ex vivo binding using [^{3}H]M-MPEP

Mice (n=5) were dosed orally (PO) with HTL0014242 in vehicle (10% DMAC, 10% Solutol HS 15 and 80% of 10% aqueous HPβCD). Two hours post-dose animals were culled by

JPET Fast Forward. Published on February 4, 2021 as DOI: 10.1124/jpet.120.000371
This article has not been copyedited and formatted. The final version may differ from this version.

cervical dislocation, followed by collection of blood by cardiac puncture. Blood was collected into EDTA-K2 tubes and centrifuged (2000 x *g*; 5 min; 4°C) to obtain plasma. Forebrains were halved along the mid-line and one half was prepared by homogenisation (Polytron Homogeniser; 7000 rpm; 20 s) in 40 volumes of binding buffer (50 mM HEPES, 150 mM sodium chloride, pH 7.5) immediately prior to use in [^{3}H]M-MPEP binding assays (following the methodology described in Christopher et al., 2015 but using 100 µL homogenate/well; 4°C; 10 min incubation, and 80 nM [^{3}H]M-MPEP (20x Kd)).

The other brain half and plasma were analysed to quantify levels of HTL0014242. The analytical methods used were identical to those described in the rat *ex vivo* binding section below.

Mouse in vivo binding using [^{3}H]M-MPEP

C57BL/6 mice were dosed with HTL0014242 (1, 3 or 10 mg/kg, PO; n=2 per dose group) or intraperitoneally (IP) (n=3 per dose group) with vehicle (10% Solutol HS 15 and 90% of 10% aqueous HPβCD). To define non-specific binding, a saturating dose of MPEP (50 mg/kg, IP) was administered. 1h post dose, [^{3}H]M-MPEP (30 µCi/kg, in water) was administered as an IV bolus via the tail vein. One minute later, mice were decapitated, brains removed, and forebrain dissected. Tissue was weighed and homogenized in 10 volumes of ice-cold homogenization buffer (10 mM potassium phosphate, 100 mM KCl, pH 7.4) using a Polytron homogenizer. Homogenates were filtered over GF/B membrane filters and washed twice with 5 mL ice-cold homogenization buffer. Filters were counted for radioactivity using a liquid scintillation counter and specific binding was calculated by subtracting the non-specific binding.

A pharmacokinetic study was conducted to determine brain and plasma exposures in the C57Bl/6 mice over the dose ranges studied for $mGlu_5$ RO. Mice were dosed with

JPET Fast Forward. Published on February 4, 2021 as DOI: 10.1124/jpet.120.000371
This article has not been copyedited and formatted. The final version may differ from this version.

HTL0014242 (1, 3 and 10 mg/kg PO or 1, 3, 10 and 30 mg/kg IP; n=3 per time point per group). Blood samples were taken at 0.25, 0.5, 1, 2, 4, 6 h post dose and plasma layer separated by centrifugation (2000 x *g*; 5 min; 4°C). The whole brain was rapidly removed and frozen on dry ice. Brains were homogenized in 10 volumes of ice-cold homogenization buffer (10 mM potassium phosphate, 100 mM KCl, pH 7.4). Following protein precipitation with acetonitrile containing an internal standard, the samples were analyzed for test compound via LC-MS/MS using a similar approach to that described in the rat *ex vivo* binding section. The concentration data at 1 mg/kg PO was below quantifiable limits and so dose proportionality was assumed to estimate exposure based on the 3 mg/kg data.

Rat ex vivo autoradiography using [^{3}H]M-MPEP

$mGlu_5$ RO was measured in brain 1 h following oral administration of HTL0014242 (1, 3, 10 mg/kg) or mavoglurant (3, 10, 30 mg/kg) in Sprague-Dawley rats (n=5 per dose group). Whole brains were removed and a coronal block containing the hippocampus was cut with one half rapidly cooled to -20/-30°C for sectioning and the other stored at -80°C to quantify compound exposure. Sections of the hippocampal CA3 region were prepared using a cryostat and incubated with [^{3}H]M-MPEP for 10 min at room temperature followed by rapid washes with ice-cold buffer. The low temperature during sample processing, short [^{3}H]M-MPEP incubation time and rapid washing were precautions taken to minimize dissociation of dosed compound from $mGlu_5$. Levels of bound radioactivity in the sections was determined using a beta imager. Specific binding (cpm/mm^2) was generated by subtraction of mean non-specific binding (cpm/mm^2) from mean total binding (cpm/mm^2) for each animal. Mean specific binding was used to determine a single RO value for each dose level as outlined below.

JPET Fast Forward. Published on February 4, 2021 as DOI: 10.1124/jpet.120.000371
This article has not been copyedited and formatted. The final version may differ from this version.

Terminal blood and halved brain samples were collected to measure compound concentrations. Blood was centrifuged at 1900 x *g* for 5 min at 4 °C to prepare plasma. Brain was homogenized in water (1:4). Protein was precipitated from 50 µL aliquots of the individual plasma or brain homogenates by adding 150 µL methanol followed by centrifugation for 30 min at 4 °C. Aliquots of the resulting supernatant were diluted 2:1 with HPLC grade water in a 96-well plate. A standard curve was prepared by spiking control plasma and brain with varying concentrations of test compound dissolved in DMSO and then treated in an identical manner to the test samples. Samples were then analysed using LC-MS/MS with electrospray ionisation set in positive mode. The system consisted of an Acquity™ Binary Solvent Manager (BSM), Acquity™ 4-position heated column manager, 2777 Ultra High Pressure Autosampler and a Xevo-TQ MS Triple Quadrupole mass spectrometer (Waters Ltd, Herts, UK). Gradient elution over 1.8 min with 10 mM ammonium formate + 0.1 % v/v formic acid in water and methanol at flow rate of 0.6 mL/min was performed. A linear regression was used to generate the calibration curve for HTL0014242. Concentrations of HTL0014242 were calculated using the peak area ratio of analyte to internal standard based on the standard curve.

Data analysis in the rodent ex vivo and in vivo occupancy assays using [^{3}H]M-MPEP

Data were expressed as % RO (data normalized to average specific binding in vehicle samples as 100% and % HTL0014242 or mavoglurant $mGlu_5$ RO, was calculated as: 100% - % [^{3}H]M-MPEP bound in the presence of drug-treated sample). For the mouse *in vivo* occupancy experiments the assay was run on three separate occasions and the receptor occupancy shown is the average receptor occupancy and standard deviation from the three combined experiments.

JPET Fast Forward. Published on February 4, 2021 as DOI: 10.1124/jpet.120.000371
This article has not been copyedited and formatted. The final version may differ from this version.

Rat in vivo PET RO study using [^{18}F]FPEB

The aim of this study was to measure $mGlu_5$ RO of HTL0014242 in the rat brain using 3[^{18}F]Fluoro5[(pyridine3yl)ethynyl]benzonitrile ([^{18}F]FPEB) PET imaging.

Anaesthesia and dosing

Rats (3 groups, n=5 per group) were administered vehicle or HTL0014242 (1 or 10 mg/kg, PO). 15 mins after dosing, the rats were anesthetized and maintained under terminal isoflurane anaesthesia (2-3% isoflurane, 1 L/min O2). Body temperature was kept stable using a heating pad. Indwelling cannulae were surgically implanted in a vein (for [^{18}F]FPEB tracer administrations) and an artery (for blood sampling of tracer kinetics). Approximately 100 IU heparin sodium was given IV prior to the scan to aid blood sampling.

PET scanning

PET imaging was performed using an Inveon DPET with docked multi-modality CT scanner. The brain was placed in the field of view of the scanner and a CT scan was acquired for attenuation and scatter correction. 1.5 h after administration of the vehicle or HTL0014242, a 60 min dynamic PET scan was acquired after the IV administration of 4-18 MBq of [^{18}F]FPEB.

Arterial sampling

To generate a [^{18}F]FPEB plasma input function continuous arterial blood samples were taken at 3 sec intervals during the first minute and discrete samples were taken across a 60 min period. Blood was collected into tubes coated with heparin. Radioactivity concentration in

JPET Fast Forward. Published on February 4, 2021 as DOI: 10.1124/jpet.120.000371
This article has not been copyedited and formatted. The final version may differ from this version.

blood and plasma were determined at all time points. Discrete plasma samples were extracted and analyzed by HPLC to determine the percentage of parent compound.

Compound exposure determination and ex-vivo [^{18}F]FPEB uptake distribution

Blood samples were collected 0, 30 and 60 min after the start of the PET scan, equating to 1.5, 2.0 and 2.5 h post HTL0014242 dose. The rats were sacrificed 60 min after [^{18}F]FPEB injection (after the PET scan) by exsanguination followed by cervical dislocation under terminal anesthetic. Brain hemispheres were separated with one half for analysis of HTL0014242 concentration. The other half was used to determine ex-vivo [^{18}F]FPEB uptake in regions of interest (ROI) to confirm HTL0014242 competed for the same mGlu$_5$ binding site as [^{18}F]FPEB.

Brain was homogenised in water (4 mL/g). Protein was precipitated from 10 μL aliquots of the individual plasma or brain homogenates by adding 100 μL acetonitrile followed by mixing (150 rpm, 20 min) and centrifugation (3000 rpm, 15 min). Aliquots of the resulting supernatant were diluted 2:1 with HPLC grade water in a 96-well plate. A standard curve was prepared by spiking control plasma and brain with varying concentrations of test compound dissolved in DMSO and then treated in an identical manner to the test samples as described above to provide a final concentration range of 1 - 5000 ng/mL (for plasma) and 2- 10000 ng/g (for brain). Samples were then analysed using UHPLC - tandem mass spectrometry using electrospray ionisation. The system consisted of a Shimadzu Nexera X2 HPLC system coupled with a Shimazdu LCMS 8060 mass spectrometer. Gradient elution over two minutes with water containing 0.1% formic acid and acetonitrile containing 0.1% formic acid at an organic at flow rate of 0.4 mL/min was performed. A linear regression was used to generate

JPET Fast Forward. Published on February 4, 2021 as DOI: 10.1124/jpet.120.000371
This article has not been copyedited and formatted. The final version may differ from this version.

the calibration curve for HTL0014242. Concentrations of HTL0014242 were calculated using the peak area ratio of analyte to internal standard based on the standard curve.

Ex-vivo distribution of [^{18}F]FPEB was determined in dissected ROIs (cortex, prefrontal cortex, hypothalamus, thalamus, hippocampus, striatum, superior and inferior colliculus, cerebellar vermis, cerebellum, and rostral and caudal medulla). Tissues were weighed and radioactivity measured using a gamma-counter to determine standardised uptake values (SUV) following vehicle, 1 mg/kg and 10 mg/kg of HTL0014242. All radioactivity counts were decay corrected to the time of tracer injection and expressed as standardized uptake value ratio. SUV was measured as:

$$SUV = \frac{Radioactivity\ concentration\left(\frac{kBq}{ml\ or\ g}\right)}{Injected\ dose\ (kBq)/(Body\ weight\ (g))}$$

A one-way ANOVA with post-hoc analysis (Tukey multiple comparisons) was used to assess dependent differences on [^{18}F]FPEB uptake in ROIs.

Image and data analysis

The PET images were acquired in list mode and reconstructed with increasing frame times over the duration of the scan to characterize the radiotracer kinetics. 3D histograms with span 3 and maximum ring difference of 79 were used. Fourier re-binning was performed, and images were reconstructed using a 2D FBP algorithm and a ramp filter and zoom of 1 to generate images on a 128 x 128 matrix. Image processing and data analysis were performed using VivoQuant™ and MIAKAT™, an in-house computational pipeline implemented in MATLAB. Regions of interest (ROI) (striatum, thalamus, hypothalamus, cerebellum, cortex, prefrontal cortex, hippocampus and “other” were defined in VivoQuant and used to generate time activity curves (TACs) in MIAKAT.

JPET Fast Forward. Published on February 4, 2021 as DOI: 10.1124/jpet.120.000371
This article has not been copyedited and formatted. The final version may differ from this version.

Using the TACs and parent plasma input function, the volume of distribution (V_T) was calculated using a two-tissue compartmental model for individual animal in each region and mean at each dose calculated. Mean V_T data were expressed as % RO by first determining % [^{18}F]FPEB bound and then normalising this to vehicle as 100% RO. Where % [^{18}F]FPEB bound = (x/vehicle VT)*100 and where % HTL0014242 occupancy = (100 - % [^{18}F]FPEB bound. Average brain $mGlu_5$ RO was determined from the mean of the RO in each region.

Cynomolgus monkey in vivo PET RO study using [^{18}F]FPEB

Anaesthesia and dosing

Cynomolgus monkeys were anaesthetised (intramuscular injection of Aflaxan 2 mg/kg, dexmedetomidine 0.02 mg/kg, and midazolam 0.3 mg/kg), intubated and maintained on oxygen and 1.5 – 2.5% isoflurane throughout the imaging sessions. PET imaging was performed on the FOCUS-220 PET scanner (Siemens Healthcare Molecular Imaging, Knoxville, TN, USA). Baseline scans were measured over 1 to 2 h in each monkey following intravenous injection of [^{18}F]FPEB over 3 min (155 MBq or 169.6 MBq for each monkey).

HTL0014242 was dosed orally as suspension, in 10% Solutol HS 15, and 9% HP-β-CD in water 2 h prior to injection of [^{18}F]FPEB (169.2 or 101.3 MBq for each monkey). Competition scans were conducted over a period of 2 h following injection of [^{18}F]FPEB. Dynamic PET scanning was preceded by transmission for attenuation and scatter correction.

Arterial sampling

The arterial plasma input functions corrected for the presence of radio-metabolites were generated for all scans based on blood samples taken from the femoral artery. Manual

JPET Fast Forward. Published on February 4, 2021 as DOI: 10.1124/jpet.120.000371
This article has not been copyedited and formatted. The final version may differ from this version.

sequential blood samples (0.5–3.5 mL) were collected at 18 selected time-points during the 120-min scan. Two 3.5 mL samples were collected before tracer administration to evaluate tracer stability in blood. Samples were collected in EDTA anticoagulant tubes and analyzed for radioactivity over time in a gamma counter (Wallac 2480 Wizard 3M Automatic γ-counter, Perkin-Elmer, Waltham, Massachusetts). Pre-tracer standards were used to evaluate the tracer ex vivo stability in blood. Plasma free fraction (fp) was determined through ultrafiltration.

Compound exposure determination

Blood samples were collected pre-dose and at 60, 120 (just prior to tracer), and 240 min (end of scan) post-dose, relative to the HTL0014242 administration. Plasma was prepared and HTL0014242 concentrations were measured by LC-MS/MS using a Shimadzu Nexera X2 HPLC system coupled with a SCIEX API 5500 Triple Quad mass spectrometer. Chromatograms were integrated using SCIEX Analyst 1.6.2 software. A linear regression was used to generate the calibration curve for HTL0014242. Concentrations of HTL0014242 were calculated using the peak area ratio of analyte to internal standard based on the standard curve.

Image and data analysis

Reconstructed PET images were analyzed using the image processing PMOD software package v3.802 (PMOD Technologies, Zurich, Switzerland). Regions of interest (VOIs) were defined on a stereotaxic anatomical cynomolgus brain atlas to which the subject's own anatomical T1 scans were registered, masks were created for the caudate, putamen, hippocampus, anterior cingulate cortex and posterior cingulate cortex, frontal cortex, temporal cortex, parietal cortex, occipital cortex and cerebellum (Ballinger et al., 2013).

JPET Fast Forward. Published on February 4, 2021 as DOI: 10.1124/jpet.120.000371
This article has not been copyedited and formatted. The final version may differ from this version.

Masks were applied to dynamic images to extract the average activity concentration (kBq/cc) within each VOI and generate time activity curves (TAC) representing regional brain activity concentration over time. TACs were expressed in standardized uptake value (SUV) units (g/mL) by normalizing by the weight of the animal and the injected dose.

A two-tissue compartmental model was used to determine the total volume of distribution (V_T) values for each brain region using metabolite-corrected plasma curves (i.e. arterial input function). A Lassen plot (Cunningham et al, 2010) analysis was performed in GraphPad Prism software and used to estimate $mGlu_5$ occupancy as described by equation: $V_T^{Baseline} - V_T^{Drug} = Occ \times (V_T^{Baseline} - V_{ND})$ which when represented graphically for each (x=V_T baseline, y=V_T baseline - V_T drug) produces a linear relationship, where the x intercept equals V_{ND} and the gradient is equal to global target occupancy. A global occupancy was determined graphically as the slope of the line. Occupancy measurements in individual brain regions were determined using the equation above and V_{ND} derived from the Lassen plot.
The relationship between percentage $mGlu_5$ occupancy and either plasma concentration or the dose of HTL0014242 were investigated with a single specific binding site (E_{max}) model with a fixed Hill slope of 1. $Occ=X/(X+K)$ where Occ is the measured $mGlu_5$ occupancy, X is either the HTL0014242 plasma concentration (in ng/mL), or the dose (in mg/kg), and K is either $EC50$ or $ED50$.

Plasma protein binding measurements

The plasma protein binding assay (in 10% plasma) was performed using a rapid equilibrium dialysis (RED) device. HTL0014242, mavoglurant and dipraglurant prepared in DMSO were added (10 µM; 0.5% DMSO final) to plasma from various species, supplied by B&K Universal, as follows: HTL0014242 mouse, rat and cynomolgus monkey; mavoglurant rat

JPET Fast Forward. Published on February 4, 2021 as DOI: 10.1124/jpet.120.000371
This article has not been copyedited and formatted. The final version may differ from this version.

and dipraglurant human. Duplicate samples were dialysed within the device against 4 mM potassium phosphate buffer containing 0.9% Na Cl, pH 7.4 for a minimum of 4 hours at 37°C.

After incubation, the contents of each plasma and buffer compartment were removed and mixed with equal volumes of control dialysed buffer or plasma as appropriate to maintain matrix similarity for bioanalysis. Plasma proteins were then precipitated by the addition of acetonitrile containing an analytical internal standard (50 ng/mL carbamazepine and 200 ng/mL reserpine), centrifuged and the supernatant removed for analysis by mass spectrometry (LC/MS/MS). Test compound was measured in both compartments by LC/MS/MS with concentrations quantified using a calibration curve prepared in assay buffer. The percentage drug bound and unbound were calculated using the following equations:

$$Fraction\ bound = \frac{total\ plasma\ concentration - total\ buffer\ concentration}{total\ plasma\ concentration}$$

$$\%\ unbound = 100 - \left(\frac{1}{\frac{dilution\ factor}{fu\ in\ diluted\ plasma}}\right) - 10 + 1)$$

Fraction unbound for basimglurant (rat, human) was determined from published plasma protein binding measurements (Lindermann, 2015).

Rat brain binding measurements

The brain homogenate binding assay (1 in 3 dilution) was performed using a RED device. HTL0014242 prepared in DMSO was added (5 µM; 0.5% DMSO final) to brain homogenate (B&K Universal) and dialysed within the device (n=2) against 4 mM potassium phosphate buffer containing 0.9% Na Cl, pH 7.4 for 4 hours at 37°C. After incubation, the contents of each homogenate and buffer compartment were removed and mixed with equal volumes of

JPET Fast Forward. Published on February 4, 2021 as DOI: 10.1124/jpet.120.000371
This article has not been copyedited and formatted. The final version may differ from this version.

control dialysed buffer or plasma as appropriate to maintain matrix similarity for bioanalysis. Brain homogenate tissue was then precipitated by the addition of acetonitrile containing an analytical internal standard (50 ng/mL carbamazepine and 200 ng/mL reserpine), centrifuged and the supernatant removed for analysis by mass spectrometry (LC/MS/MS). Test compound was measured in both compartments by LC/MS/MS with concentrations quantified using a calibration curve prepared in assay buffer. The percentage drug bound and unbound were calculated using the following equations:

$$fraction\ bound = \frac{brain\ homogenate\ concentration - buffer\ cocentration}{brain\ homogenate\ concentration}$$

$$\%\ unbound\ in\ plasma = 100 - \left(\frac{1}{\frac{dilution\ factor}{fu\ in\ brain\ homogenate}} \right) - dilution\ factor + 1$$

Fraction unbound in rat brain for mavoglurant was estimated from cerebro-spinal fluid (CSF) as a fraction of total brain concentration from exposure reported in Bennett, 2014. A similar approach was used to determine unbound fraction in rat brain for dipraglurant as determined in a separate PK study (unpublished). For basimglurant an average brain fu was computed from the cited rat brain/plasma ratio (Kp 1.7-2.9), unbound fraction in plasma (0.021) and assuming good passive brain penetration consistent with unbound brain/unbound plasma, Kpuu = 1 (Lindermann 2015) whereby brain fu = Kpuu* plasma fu/Kp. It was assumed the fraction unbound in brain was consistent across species.

Additional characterization of $mGlu_5$ NAMs

The following data and data manipulations were used for calculating the exposure-receptor occupancy for dipraglurant, mavoglurant and basimglurant.

JPET Fast Forward. Published on February 4, 2021 as DOI: 10.1124/jpet.120.000371
This article has not been copyedited and formatted. The final version may differ from this version.

Dipraglurant: Human exposure data from Tison et al., 2016; Day 1 50 mg C_{max} plasma (793.4 ng/ml) data was normalized to reflect the exposure at 100, 200 and 300 mg where RO was measured. This day 1 predicted exposure is consistent with the cited exposure following repeat dosing at 100 mg (C_{max} plasma 1682.8 ng/ml) since no accumulation would be expected for the short half-life observed. RO data from Addex Therapeutics Initiating Report, 2016, Wong et al., 2018[b].

Mavoglurant: Rodent exposure and RO was taken from Bennett et al., 2014.

Basimglurant: Rat RO from Lindermann et al, 2015. Human day 1 plasma exposure and median pharmacokinetic half-life in Major Depressive Disorder patients taken from Cosson 2018 and $mGlu_5$ receptor occupancy estimated at steady state (Quiroz 2016). Given the recognized long half-life of this compound it was necessary to estimate the steady state C_{max}, by calculating an accumulation ratio using the following equation.

$$\frac{1}{1 - e^{(-elimination\ rate\ constant \times dosing\ interval)}}$$

Where elimination rate constant =0.693/quoted half-life of 49h.

This accumulation ratio (3.5) was then applied to the C_{max} quoted on day 1 in order to correlate the steady state exposure and receptor occupancy. The plasma exposure was used to estimate unbound brain concentration taking account of Kp and unbound fraction in brain.

Predicting RO using a simple E_{max} model

A simple E_{max} model was used to predict receptor occupancy as follows:

$$mGlu5\ inhibition = concentration \times \frac{100}{Ki + concentration}$$

JPET Fast Forward. Published on February 4, 2021 as DOI: 10.1124/jpet.120.000371
This article has not been copyedited and formatted. The final version may differ from this version.

Where concentration was either unbound plasma or unbound brain concentration.

Unbound concentrations were computed by taking measured concentration * unbound fraction as determined in plasma or brain tissue. For mavoglurant, measured CSF concentrations were considered to represent unbound brain concentrations.

Statistical analyses

Where there are multiple measurements, data is presented as mean ± standard deviation. Exposure-RO data was fitted to a variable-slope four parameter fit (GraphPad Prism version 8), with basal constrained to '0' and top constrained to '100'. An Anova F-Test was conducted to determine whether the resulting Hill Slope was significantly different to 1.

JPET Fast Forward. Published on February 4, 2021 as DOI: 10.1124/jpet.120.000371
This article has not been copyedited and formatted. The final version may differ from this version.

Results

The physicochemical properties, $mGlu_5$ affinity, human plasma pharmacokinetic half-life and rat brain penetration properties of HTL0014242, dipraglurant, mavoglurant and basimglurant are described in **Table 1.** $mGlu_5$ affinity varies by approximately 260-fold between compounds, with HTL0014242 and basimglurant having the highest $mGlu_5$ NAM affinity. $mGlu_5$ affinity was shown to be very consistent across species. Partitioning into brain was measured in the rat for HTL0014242, dipraglurant and mavoglurant indicating approximately 17-fold variation in Kp and 4-fold variation in the estimated Kpuu with HTL0014242 having the highest relative brain penetration. The precise Kpuu is unknown for basimglurant but assumed to be close to 1 given the cited good brain penetration (Lindermann, 2015).

Total brain and plasma exposure for HTL0014242 in mouse and rat are shown in **Table 2**. Exposures are taken at the same time point as when $mGlu_5$ RO is measured. For PET studies, assessment of ex-vivo [^{18}F]FPEB biodistribution confirmed HTL0014242 competed for the same binding site as [^{18}F]FPEB. Drug concentrations were measured at the start of the [^{18}F]FPEB scan in order to reflect the highest exposure. However, it should be noted that previous pharmacokinetic studies showed measurements of exposure to be similar over the same time period as used in this PET study (unpublished data). Plasma exposure and brain exposure for mavoglurant in the rat, basimglurant in rat and human and dipraglurant in human are given in **Table 3**. Brain exposure for basimglurant and dipraglurant in human was estimated assuming the same partitioning as for rat. For dipraglurant dose proportionality was assumed to estimate exposures at the higher doses of 200 and 300 mg where $mGlu_5$ RO has been measured.

The $mGlu_5$ RO measured and the dose and exposure levels are illustrated in **Tables 2** and **3**. $mGlu_5$ RO increased with increasing dose/exposure for all compounds studied, where

JPET Fast Forward. Published on February 4, 2021 as DOI: 10.1124/jpet.120.000371
This article has not been copyedited and formatted. The final version may differ from this version.

multiple dose levels were profiled. For each compound there are clear exposure-RO relationships across a range of species but when the data is plotted together the relationship for each compound is distinct, with greater than 100-fold difference between the exposures required for a similar level of RO (i.e. not overlaying) as illustrated in **Figure 1A.** When both the unbound concentration in plasma and $mGlu_5$ affinity are accounted for, as illustrated in **Figure 1B,** the exposure-response relationships for each compound do appear to be closer together although greater than 10-fold difference was found between the most and least potent relationships.

Figure 1C shows when considering differences in both the unbound concentration in brain and $mGlu_5$ affinity the relationship between compounds and RO is more unified, with exposure-RO relationships being <10-fold separated. Fitting the data to a variable-slope four parameter fit (GraphPad Prism version 8) resulted in a curve with EC_{50} calculated to be 0.67 (confidence interval 0.41-1.10) with a Hill slope of 0.81 (confidence interval 0.38 -1.23), which was demonstrated to be not significantly different from 1 based on an F-test. The F-test comparison of data fits (null hypothesis Hill slope = 1 versus an alternative unconstrained Hill slope) indicated that Hill slope = 1 produced the better fit ($p = 0.4$, F ratio = 0.74). The theoretical exposure-RO relationship is shown in **Figure 1C** in the dotted line, where 50% $mGlu_5$ RO is achieved where ratio of unbound brain concentration/K_i = 1. Both the theoretical curve and the curve fit of the data are remarkably similar, given the breadth of compounds and datasets used for the analysis.

HTL0014242 predictions of RO from unbound plasma or brain are given in **Table 4** and a graphical representation of the predictions from unbound plasma versus measured RO are given in **Figure 2**. The predictions from either matrix are similar and consistent with the good brain penetration observed for this compound in the rat (Kpuu = 1.3; **Table 1)**. **Figure 2** does demonstrate a tendency to underpredict $mGlu_5$ RO across all species when predicting from

JPET Fast Forward. Published on February 4, 2021 as DOI: 10.1124/jpet.120.000371
This article has not been copyedited and formatted. The final version may differ from this version.

plasma exposure with predictions being from 8% higher to 41% lower than measured with an average underprediction of 14%. **Table 5** illustrates predictions of RO for mavoglurant, dipraglurant and basimglurant and indicates similar RO or slight overprediction of observed RO for these compounds.

JPET Fast Forward. Published on February 4, 2021 as DOI: 10.1124/jpet.120.000371
This article has not been copyedited and formatted. The final version may differ from this version.

Discussion

The current study is the first to formally investigate exposure-RO relationships of selective $mGlu_5$ NAMs across species in a collective manner. This investigation clearly demonstrated that, irrespective of species, a more unified exposure-response relationship across $mGlu_5$ NAMs was evident when accounting for unbound brain concentration and $mGlu_5$ affinity, rather than total systemic exposure. Consideration is given to whether RO could be predicted for a given level of exposure, with the potential to underpin future clinical trial designs. The strengths and limitations of these approaches are highlighted in this discussion.

Dipraglurant, mavoglurant, basimglurant and HTL0014242 have all progressed to clinical development despite having distinct structures and physiochemical attributes, which contribute to differing pharmacokinetic properties and $mGlu_5$ receptor affinities ranging from K_i values of 0.56 to 117 nM. These NAMs are all selective for $mGlu_5$ (Lindermann et al., 2015; Christopher et al., 2015; Vranesic et al., 2014; Bezard et al., 2014), have no known active metabolites and all bind to the M-MPEP site. Furthermore, the current study demonstrated that their affinities are conserved across human, mouse, rat and monkey $mGlu_5$ orthologues, consistent with previously reported data for basimglurant (Lindermann et al., 2015). In combination this data set is uniquely placed to examine cross-species exposure-RO relationships across $mGlu_5$ NAMs with differential physiochemical properties.

The relationship between total plasma exposure and $mGlu_5$ RO demonstrated distinct exposure-RO profiles for each compound, as illustrated by the oral dose of 3 mg/kg in the rat, where HTL0014242 demonstrated 80% $mGlu_5$ RO whereas mavoglurant produced 45% RO despite similar plasma concentrations of 139 and 128 ng/ml, respectively. The free drug hypothesis states that only unbound compound binds the target, therefore correcting to unbound plasma concentration and compound affinity improved the exposure-occupancy

JPET Fast Forward. Published on February 4, 2021 as DOI: 10.1124/jpet.120.000371
This article has not been copyedited and formatted. The final version may differ from this version.

relationship compared to total plasma alone. As $mGlu_5$ RO is measured in the brain, it is not surprising that the most unified exposure-RO relationship emerges when unbound brain concentrations are accounted for as well as $mGlu_5$ affinity. The fit of the data indicated that the Hill slope was not significantly different from 1, indicating that $mGlu_5$ RO likely reflects binding at a single receptor binding site. Consequently, this unified relationship spans the theoretical curve predicted from a simple E_{max} model, with a Hill slope of 1 and where an unbound exposure/K_i ratio of 1 would be expected to yield 50% RO. This observation is consistent with the published dipraglurant human plasma exposure-RO relationship, which obeyed a first order Hill equation (Wong et al., 2018[b]). Given the number of data sources for the present analysis, covering a range of species and $mGlu_5$ NAMs with differing properties, it is remarkable that the exposure-RO relationships are so close.

However, whilst a more unified relationship is achieved by using unbound brain corrected for $mGlu_5$ affinity to relate to RO, there is still up to 10-fold variance in exposure relative to K_i for a given level of RO. Therefore, it is important to consider the key factors which may contribute to this variance, namely measurement of brain penetration, free fraction and associated experimental design and methodology for determination of exposure and RO.

Firstly, understanding brain penetration is essential but challenging since the concentrations can be influenced by technical factors such as whether brain exposure is derived from CSF or whole brain measurements (Westerhout et al., 2011; O'Brown et al., 2018). In this study, brain penetration was assessed using total brain concentrations, fraction unbound in rodent brain homogenate and, in one case, CSF concentrations. Observations with mavoglurant using CSF data were consistent with the overall exposure-RO relationships indicating that any bias was minimal. Furthermore, for the compounds studied here, the Kpuu observed in rodents were consistent with largely passive distribution, which provided confidence in extrapolation across species.

JPET Fast Forward. Published on February 4, 2021 as DOI: 10.1124/jpet.120.000371
This article has not been copyedited and formatted. The final version may differ from this version.

It was assumed that the degree of brain partitioning of dipraglurant and basimglurant was equivalent to that observed in the rat. The brain unbound/K_i-RO relationship was fitted excluding the human data and this confirmed a similar EC_{50} and Hill slope to that observed with the full dataset (EC_{50} = 0.49 (95% confidence interval 0.28-0.84); Hill slope = 0.86 (95% confidence interval 0.41-1.31)), confirming that the overall relationship was not biased by the assumption that human and rat brain penetration was similar for these compounds.

A second factor which may influence variance in exposure-RO relationship is the method used to assess the true unbound concentration available to interact with the target. The established *in vitro* methods for measuring brain unbound fraction are crude, relying on whole brain homogenate with no indication of variance in unbound concentrations across brain regions. For passively permeating compounds such as HTL0014242, the unbound plasma concentration would be expected to reflect unbound brain concentration, allowing the use of unbound fraction in plasma as a surrogate. Based on the above observation that these exposure-RO relationships are consistent with a simple E_{max} model, it was deemed valid to apply this methodology to predicting RO from either matrix, brain or plasma. HTL0014242 underpredicted the measured $mGlu_5$ RO by an average of 14% based on brain data. Given the similarity in prediction from the two matrices, there is most likely an underestimate of free fraction rather than brain penetration, especially for HTL0014242 due to its high plasma protein and brain tissue binding (>99% bound) whereby it is challenging to accurately measure low unbound concentrations (<1% unbound). Using this approach for dipraglurant, mavoglurant and basimglurant, RO tends to be similar or overpredicted compared to measured RO. Since these compounds vary in brain penetration, but all have higher unbound fraction than HTL0014242, this observation highlights the challenge in accurately predicting RO from unbound concentrations when binding is high.

JPET Fast Forward. Published on February 4, 2021 as DOI: 10.1124/jpet.120.000371
This article has not been copyedited and formatted. The final version may differ from this version.

Despite the slight underprediction of RO based on animal data, HTL0014242 illustrates that this approach could be used to provide a conservative estimate of $mGlu_5$ RO across a variety of species including human. Measurement of HTL0014242 $mGlu_5$ RO in human would be a useful next step to determine whether the relationship observed in animals is consistent with human and how plasma concentrations relate to $mGlu_5$ RO in the brain. Despite the caveats around the influence of free fraction, predicted RO for these compounds are in line with observed values, supporting the use of unbound plasma concentrations measured clinically to estimate RO. Such information could aid dose selection and clinical experimental design providing that the relationship between unbound plasma and unbound brain concentrations is understood.

Experimental design factors relating to the dose selection, sampling time for measurement of exposure versus RO and number of replicates could potentially contribute to the overall variability in the exposure-RO relationships. For new experimental data, doses were deliberately chosen to support determining a full exposure-RO relationship. For *in vivo* and *ex vivo* RO measurements, the exposure was measured from the same brain sample as that used for RO, thus removing any potential disconnect between measurements. For PET studies, the scan time for HTL0014242 studies was 1 h in duration but plasma and brain concentrations were known to be similar across this period following oral dosing. Scanning periods are not reported for dipraglurant and basimglurant but the long half-life of basimglurant suggests that brain concentrations would remain consistent. Dipraglurant has a short half-life in humans (<1 h), so it is possible that the C_{max} measured exposure overestimates the average concentration associated with the RO. However, considering the large dataset containing compounds with different properties, it is unlikely that the timing of exposure and $mGlu_5$ RO measurements contributed significantly to the variance in exposure-RO relationships. The number of replicates for HTL0014242 RO and exposure studies was

JPET Fast Forward. Published on February 4, 2021 as DOI: 10.1124/jpet.120.000371
This article has not been copyedited and formatted. The final version may differ from this version.

relatively small (2-5) but adequate considering the data was part of a larger dataset covering a wide range of $mGlu_5$ RO (12-95%). Lastly, in the cynomolgus PET study, only one monkey was used for each dose level since RO could be related directly to exposure measured in that animal. Although the exposure-RO relationship was consistent with that observed in other species, it is possible that increasing the number of replicates would improve the accuracy and precision of this data. A further consideration relates to the methodology used to measure $mGlu_5$ RO. $mGlu_5$ NAM PET studies have used a variety of PET ligands. Whilst there is potential for ligands to bind at different binding sites, it has been established that similar chemical scaffolds can inhibit prototypic MPEP/FPEB sites by interacting at non-identical but overlapping sites (Gregory et al., 2014[b], Rook et al., 2015) and [^{18}F]FPEB or [^{11}C]ABP688 PET ligands appear to bind at the M-MPEP binding site (Hamill et al., 2005; Wyss et al., 2007; Hintermann et al., 2007). Therefore, it is unlikely that the choice of PET ligand contributes to the variance observed in the exposure-RO relationships.

PET studies provide distribution and derived ligand binding across several brain regions. HTL0014242 RO ranged from 62.2 to 79.1% at 1 mg/kg and 73.3 to 89.1% at 10 mg/kg in 4 key regions (striatum, cerebellum, frontal cortex and hippocampus) in the rat. However, this level of variance is insufficient to explain an underprediction of RO. The widespread expression of $mGlu_5$ (Hovelsø et al., 2012; Ferraguit et al., 2006) would suggest a consistent RO across the brain, supporting the use of total RO to compare to exposure. It should also be noted that there was some inter-animal variability in measured $mGlu_5$ RO, as indicated by the standard deviations quoted. As the predicted ROs for HTL0014242 fall within this level of variability (**Table 3**), the most likely explanation for underprediction is in the estimate of unbound faction as described above.

A strength of this study is that every effort was taken to minimize the impact of factors acknowledged to contribute to variability in this novel combined analysis of new and

published data. In particular, brain penetration was measured in sufficient replicates to provide an average view of the exposure and where possible, exposure was obtained from the same animals where RO was measured. $mGlu_5$ NAMs were included which were known to bind to the same MPEP site. RO data was generated using established methods and validated $mGlu_5$ probes to provide consistency with RO incorporated from publications. Finally, for exposure and RO studies, doses were chosen to explore the full exposure-RO curve.

Despite the variability in the exposure-RO relationships, the evidence presented here suggests that the behaviour of selective $mGlu_5$ NAMs is consistent with a simple E_{max} model, thus providing guidance on extrapolation from animal to human. As more data become available, particularly in human, it would be beneficial to further expand these relationships and to encompass $mGlu_5$ NAMs with different binding modes. Notwithstanding the long history of the $mGlu_5$ field, this unified assessment of the exposure-RO relationship across species and $mGlu_5$ NAMs has demonstrated, for the first time, the importance of understanding the concentration in the target organ for the interpretation and design of nonclinical and clinical studies.

JPET Fast Forward. Published on February 4, 2021 as DOI: 10.1124/jpet.120.000371
This article has not been copyedited and formatted. The final version may differ from this version.

Acknowledgements

The authors thank John Christopher, Sarah Bucknell, Miles Congreve, James Hagan and Eimear Howley as well as colleagues in the Medicinal Chemistry and DMPK departments at Sosei Heptares for unlabeled compound synthesis, management of *in vivo* pharmacokinetic studies and/or general advice. In addition the authors also thank RenaSci Ltd for conducting the rat *ex vivo* binding studies and Ian Brown and colleagues at Teva Pharmaceuticals, 145 Brandywine Pkwy, West Chester, PA 19380, United States for mouse *ex vivo* binding studies, Ilan Rabinar, Lisa Wells and colleagues at Invicro, Hammersmith hospital, Du Cane Road, UK for conducting the rat [^{18}F]FBEP PET study, Khanum Ridler and colleagues at Invicro, New Haven, CT, US for the cynomolgus monkey [^{18}F]FBEP PET study and Graham Hagger at Royal Veterinary College, London for help with the mouse *ex vivo* binding studies.

JPET Fast Forward. Published on February 4, 2021 as DOI: 10.1124/jpet.120.000371
This article has not been copyedited and formatted. The final version may differ from this version.

Authorship Contributions

Participated in research design: Cooper, Bennett

Conducted experiments: Bennett, Sergeev, MacSweeney, Bakker

Performed data analysis: Cooper, Bennett, Sergeev

Wrote or contributed to the writing of the manuscript: Cooper, Bennett, Sergeev, MacSweeney, Bakker

References

Able SL, Fish RL, Bye H, Booth L, Logan YR, Nathaniel C, Hayter P and Katugampola SD (2011) Receptor localization, native tissue binding and *ex vivo* occupancy for centrally penetrant P2X7 antagonists in the rat. *Br J Pharmacol* **162**: 405–414.

Addex Therapeutics Initiating Report (2016) *Life Science Capital* 19 July 2016 https://www.lifescicapital.com/company/addex-therapeutics/

Anderson JJ, Rao SP, Rowe B, Giracello DR, Holtz G, Chapman DF, Tehrani L, Bradbury MJ, Cosford NDP and Varney MA (2002) [^{3}H]Methoxymethyl-3-[(2-methyl-1,3-thiazol-4-yl)ethynyl]pyridine binding to metabotropic glutamate receptor subtype 5 in rodent brain: *in vitro* and *in vivo* characterization. *J Pharmacol Exp Ther* **303**: 1044-1051.

Ametamey SM, Treyer V, Streffer J, Wyss MT, Schmidt M, Blagoev M, Hintermann S, Auberson Y, Gasparini F, Fischer UC and Buck A (2007) Human PET studies of metabotropic glutamate receptor subtype 5 with ^{11}C-ABP688. *J Nucl Med* **48**: 247–252.

Archer T and Garcia D (2016) Attention-deficit/hyperactivity disorder: focus upon aberrant N-methyl-D-aspartate receptors systems. *Curr. Top. Behav. Neurosci.* **29**: 295–311.

Ballanger, B, Tremblay L, Sgambato-Faure V, Beaudoin-Gobert M, Lavenne F, Le Bars D and Costes N (2013) A multi-atlas based method for automated anatomical Macaca fascicularis brain MRI segmentation and PET kinetic extraction. *Neuroimage* **77**: 26–43.

Bennett K, Christopher JA, Brown AJH and Marshall FH (2014) Pharmacology of mavoglurant, a metabotropic glutamate receptor 5 negative allosteric modulator. *Proceedings of the British Pharmacological Society*, Leicester University BPS Focus Meeting on Cell Signalling 013P.

Berthele A, Platzer S, Laurie DJ, Weis S, Sommer B, Zieglgänsberger W, Conrad B and Toelle T (1999) Expression of metabotropic glutamate receptor subtype mRNA (mGluR1–8) in human cerebellum. *Neuroreport* **10:** 3861-3867.

Bezard E; Pioli E; Li Q, Girard F, Mutel V, Keywood C, Tison F, Rascol O and Poli SM (2014) The mGluR$_5$ negative allosteric modulator dipraglurant reduces dyskinesia in the MPTP macaque model. *Mov Disord* **29:** 1074-1079.

Christopher JA, Aves SJ, Bennett KA, Doré AS, Errey JC, Jazayeri A, Marshall FH, Okrasa K, Serrano-Vega MJ, Tehan BG, Wiggin GR and Congreve M (2015) Fragment and Structure-Based Drug Discovery for a Class C GPCR: Discovery of the mGlu$_5$ Negative Allosteric Modulator HTL14242 (3Chloro-5-[6-(5-fluoropyridin-2-yl)pyrimidin-4-yl]benzonitrile) *J Med Chem* **58:** 6653-6664.

Cosson V, Schaedeli-Stark F, Arab-Alameddine M, Chavanne C, Guerini E, Derks M and Mallalieu NL (2018) Population Pharmacokinetic and Exposure-dizziness Modeling for a Metabotropic Glutamate Receptor Subtype 5 Negative Allosteric Modulator in Major Depressive Disorder Patients. *Clin Transl Sci* **11:** 523–531.

Cunningham VJ, Rabiner EA, Slifstein M, Laruelle M and Gunn RN (2010) Measuring drug occupancy in the absence of a reference region: the Lassen plot re-visited. *J Cereb Blood Flow Metab* **30**: 46-50.

DeLorenzo C, Gallezot JD, Gardus J, Yang J, Planet B, Nabulsi N, Ogden RT, Labaree DC, Huang YH, J John Mann3, Gasparini F, Lin X, Javitch JA, Parsey RV, Carson RE and Esterlis I (2017) *In vivo* variation in same-day estimates of metabotropic glutamate receptor subtype 5 binding using [^{11} C]ABP688 and [^{18} F]FPEB. *J Cereb Blood Flow Metab* **37:** 2716-2727.

Doré AS, Okrasa K, Patel JC, Serrano-Vega M, Bennett K, Cooke RM, Errey JC, Jazayeri A, Khan S, Tehan B, Weir M, Wiggin GR and Marshall FH (2014) Structure of class C GPCR metabotropic glutamate receptor 5 transmembrane domain. *Nature* **511**: 557-62.

Emmitte K (2013) mGlu$_5$ negative allosteric modulators: a patent review (2010-2012). *Expert Opin. Ther. Pat*. **23:** 393-408.

Ferraguti F and Shigemoto R (2006) Metabotropic glutamate receptors. *Cell Tissue Res* **326:** 483504.

Fridén M, Wennerberg M, Antonsson M, Sandberg-Ställ M, Farde L and Schou M (2014) Identification of positron emission tomography (PET) tracer candidates by prediction of the target-bound fraction in the brain. *EJNMMI Res* **4**: 50.

Gasparini F, Andres H, Flor PJ, Heinrich M, Inderbitzin W, Lingenhöhl K, Müller H, Munk VC, Omilusik K, Stierlin C, Stoehr N, Vranesic I and Kuhn R (2002) [^{3}H]-M-MPEP, a Potent, Subtype-Selective Radioligand for the Metabotropic Glutamate Receptor Subtype 5. *Bioorg Med Chem Lett* **12:** 407-409.

Gregory KJ, Dong EN, Meiler J and Conn PJ (2011)[a] Allosteric modulation of metabotropic glutamate receptors: Structural insights and therapeutic potential. *Neuropharmacology* **60:** 6681.

Gregory KJ, Nguyen ED, Malosh C, Mendenhall JL, Zic JZ, Bates BS, Noetzel MJ, Squire EF, Turner EM, Rook JM, Emmitte KA, Stauffe SR, Lindsley CW, Meile J and Conn PJ (2014)[b] Identification of specific ligand-receptor interactions that govern binding and cooperativitiy of diverse modulators to a common metabotropic glutamate receptor 5 allosteric site. *ACS Chem Neurosci* **5:** 282-295.

Haas LT, Salazar SV, Smith LM, Zhao HR, Cox TO, Herber CS, Degnan AP, Balakrishnan A, Macor JE, Albright CF, and Strittmatter SM (2017) Silent Allosteric Modulation of mGluR5 Maintains Glutamate Signaling while Rescuing Alzheimer's Mouse Phenotypes. *Cell Rep* **20:** 76-88.

Hamill T, Krause S, Ryan C, Bonnefous C, Govek S, Seiders TJ, Cosford NDP, Roppe J, Kamenecka T, Patel S, Gibson RE, Sanabria S, Riffel K, Eng W, King C, Yang Z, Green MD, O'Malley SS, Hargreaves R and Burns HD (2005) Synthesis, Characterization, and

First Successful Monkey Imaging Studies of Metabotropic Glutamate Receptor Subtype 5 (mGluR5) PET Radiotracers. *Synapse* **56**: 205–216.

Hamilton A, Vasefi M, Vander Tuin CV, McQuaid RJ, Anisman H and Ferguson SSG (2016) Chronic Pharmacological mGluR5 Inhibition Prevents Cognitive Impairment and Reduces Pathogenesis in an Alzheimer Disease Mouse Model. *Cell Rep* **15**: 1859-1865.

Hintermann S, Vranesic I, Allgeier H, Brülisauer A, Hoyer D, Lemaire M, Moenius T, Urwyler S, Whitebread S, Gasparini F and Auberson YP (2007) ABP688, a novel selective and high affinity ligand for the labelling of $mGLu_5$ receptors: identification, *in vitro* pharmacology, pharmacokinetic and biodistribution studies. *Bioorg Med Chem* **15:** 903-914.

Hovelsø N, Sotty F, Montezinho1 LP, Pineiro PS, Herrik KF and Mørk A (2012) Therapeutic Potential of Metabotropic Glutamate Receptor Modulators. *Current Neuropharmacology* **10:** 12-48.

Jaso BA, Niciu MJ, Iadarola ND, Lally N, Richards EM, Park M, Ballard ED, Nugent AC, Machado-Vieira R and Zarate CA (2017) Therapeutic Modulation of Glutamate Receptors in Major Depressive Disorder. *Current Neuropharmacology* **15**: 57-70.

Kazim SF, Chuang S-C, Zhao W, Wong RKS, Bianchi R and Iqbal K (2017) Early-Onset Network Hyperexcitability in Presymptomatic Alzheimer's Disease Transgenic Mice Is Suppressed by Passive Immunization with Anti-Human APP/Aβ Antibody and by mGluR5 Blockade. *Front Aging Neurosci.* **9:** 1-17.

Kågedal M, Cselényi Z, Nyberg S, Raboisson P, Ståhle L, Stenkrona P, Varnäs K, Halldin C, Hooker AC and Karlsson MO (2013) A positron emission tomography study in healthy volunteers to estimate mGluR5 receptor occupancy of AZD2066 - estimating occupancy in the absence of a reference region. *Neuroimage* **82:** 160-169.

Kalliomäki J, Huizar K, Kågedal M, Hägglöf B and Schmelz M (2013) Evaluation of the effects of a metabotropic glutamate receptor 5-antagonist on electrically induced pain and central sensitization in healthy human volunteers. *Eur J Pain* **17:** 1465–1471.

Liang SH, Yokell DL, Jackson RN, Rice PA, Callahan R, Johnson KA, Alagille D, Tamagnan G, Collier TL, Vasdev N (2014) Microfluidic continuous-flow radiosynthesis of [^{18}F]FPEB suitable for human PET imaging. *Medicinal Chemistry Communication* **5:** 432-435.

Lindemann L, Porter RH, Scharf SH, Kuennecke B, Bruns A, von Kienlin M, Harrison AC, Axel Paehler A, Christoph Funk C, Andreas Gloge A, Manfred Schneider M, Neil J. Parrott NJ, Polonchuk L, Niederhauser U, Morairty SR, Kilduff TS, Vieira E, Kolczewski S, Wichmann J, Hartung T, Honer M, Borroni E, Moreau JL, Prinssen E, Spooren W, Wettstein JG, and Jaeschke G (2015) Pharmacology of Basimglurant (RO4917523, RG7090), a Unique Metabotropic Glutamate Receptor 5 Negative Allosteric Modulator in Clinical Development for Depression. *J Pharm Exp Ther* **353:** 213-233.

Lindsley CW and Stauffer SR (2013) Metabotropic glutamate receptor 5-positive allosteric modulators for the treatment of schizophrenia (2004-2012). *Pharm Pat Anal.* **2:** 93-108.

Lohith T, Tetsuya Tsujikawa T, Simeon FG , Veronese M, Zoghbi SS , Lyoo CH , Kimura Y, Cheryl L Morse CL , Pike VW , Fujita M and Innis RB (2017) Comparison of two PET radioligands, [11C]FPEB and [11C]SP203, for quantification of metabotropic glutamate receptor 5 in human brain. *Journal of Cerebral Blood Flow & Metabolism* **37**: 2458-2470.

NCT 01348087 Long-term, Safety, Tolerability and Efficacy Study of AFQ056 in Adult Patients With Fragile X Syndrome 25 May 2016. www. Clinical.trials.gov.

NCT 01348087 Long-term, Safety, Tolerability and Efficacy Study of AFQ056 in Adult Patients With Fragile X Syndrome 25 May 2016. www. Clinical.trials.gov.

NCT 01483469 Human Proof of Concept Study for [11C]-RO5011232 as Radiotracer and Study of the Binding of RO4917523 to Human $mGlu_5$ Brain Receptor at Steady-State in Healthy Volunteers 1 Dec 2011. www. Clinical.trials.gov.

Newell KA and Matosin N (2014) Rethinking metabotropic glutamate receptor 5 pathological findings in psychiatric disorders: implications for the future of novel therapeutics. *BMC Psychiatry* **14:** 1-6.

O'Browm N, Pfau S and Chenghua G (2018) Bridging barriers: a comparative look at the blood-brain barrier across organisms. *Genes and Development* **32**: 466–478.

Pagano A, Rűegg D, Litschig S, Stoehr N, Stierlin C, Heinrich M, Floersheim P, Prezėau L, Carrolli F, Pini JP, Cambria A, Ivo Vranesic I, Flor PJ, Gasparini F and Kuhn R (2000) The non-competitive antagonists 2-methyl-6-(phenylethynyl)pyridine and 7-hydroxyiminocyclopropan[b]chromen-1a-carboxylic acid ethyl ester interact with overlapping binding pockets in the transmembrane region of group I metabotropic glutamate receptors. *J Biol Chem.* **275**: 33750-33758.

Patel S, Hamill TG, Connolly BM, Jagoda E, Li W and Gibson RE (2007) Species differences in mGluR5 binding sites in mammalian central nervous system determined using in vitro binding with [18F]F-PEB. *Nucl Med Biol.* **34**: 1009-1017.

Porter RHP, Jaeschke G, Spooren W, Ballard TM, Büttelmann B, Kolczewski S, Peters JU, Prinssen E, Wichmann J, Vieira E, Mühlemann A, Gatti S, Mutel V and Malherbe P (2005) Fenobam: A Clinically Validated Nonbenzodiazepine Anxiolytic Is a Potent, Selective, and Noncompetitive $mGlu_5$ Receptor Antagonist with Inverse Agonist Activity. *J Pharmacol Exp Ther* **315:** 711-721.

Quiroz JA, Tamburri P, Deptula D, Banken L, Beyer U, Rabbia M, Parkar N, Fontoura P and Santarelli L (2016) Efficacy and Safety of Basimglurant as Adjunctive Therapy for Major Depression A Randomized Clinical Trial. *JAMA Psychiatry* **73:** 675-684.

Robertson N, Jazayeri A, Errey, J, Baig A, Hurrell E, Zhukov A, Langmead CJ, Weir M and Marshall FH (2011) The properties of thermostabilised G protein-coupled receptors (StaRs) and their use in drug discovery. *Neuropharmacology* **60:** 36-44.

Rook JM, Tantawy MN, Ansari MS, Felts AS, Stauffer SR, Emmitte KA, Kessler RM, Niswender CM, Daniels JS, Jones CK, Lindsley CW and Conn PJ (2015) Relationship between *in vivo* receptor occupancy and efficacy of metabotropic glutamate receptor subtype 5 allosteric modulators with different *in vitro* binding profile. *Neuropsychopharmacology* **40:** 755-765.

Sergeev E, Howley EM, Bennett KA, Bestwick M and Barnes M (2018) Development of an Ex Vivo Receptor Occupancy Assay for the Class C GPCR mGlu$_5$. *7th BPS Focused Meeting on Cell Signalling, 16-17 April, Nottingham.*

Slassi A, Isaac M, Edwards L, Minidis A, Wensbo D, Mattsson J, Nilsson K, Raboisson P, McLeod D, Stormann T, Hammerland L and Johnson E (2005) Recent Advances in Non-Competitive mGlu$_5$ Receptor Antagonists and their Potential Therapeutic Applications *Current Topics in Medicinal Chemistry* **5**: 897-911.

Stephenson, NA, Holland, JP, Kassenbrock A, Yokell DL, Livni E, Liang SH and Vasdev N (2015) Iodonium ylide-mediated radiofluorination of 18F-FPEB and validation for human use. *J Nucl Med* **56:** 489–492.

Stocchi MD, Rascol O, Destee A, Hattori N, Hauser RA, Lang AE, Poewe W, Stacy M, Tolosa E, Gao H, Nagel J, Merschhemke M, Graf A, Kenney C and Trenkwalder C (2013) AFQ056 in Parkinson Patients With Levodopa-Induced Dyskinesia: 13-Week, Randomized, Dose-Finding Study *Mov Disord* **28**: 1838-1846.

Sullivan JM, Lim K, Labaree D, Lin SF, McCarthy TJ, Seiby JP, Tamagnan G, Huang Y, Carson RE, Ding YS and Morris ED (2013) Kinetic analysis of the metabotropic glutamate subtype 5 tracer [^{18}F]FPEB in bolus and bolus-plus-constant-infusion studies in humans *Journal of Cerebral Blood Flow & Metabolism* **33:** 532–541.

Tison F, Keywood C, Wakefield M, Durif F, Corvol JC, Eggert K, Lew M,Isaacson S, Bezard E, Poli S-M, Goetz CG, Trenkwalder C, Rascol O (2016) A Phase 2A Trial of the Novel mGluR5-Negative Allosteric Modulator Dipraglurant for Levodopa-Induced Dyskinesia in Parkinson's Disease. *Mov Disord* **31:** 1373–1380.

Trenkwalder C, Stocchi F, Poewe W, Dronamraju N, Kenney C, Shah A, von Raison F and Graf A (2016) Mavoglurant in Parkinson's Patients With L-Dopa-Induced Dyskinesias: Two Randomized Phase 2 Studies. *Mov Disord* **31:** 1054-8.

Varlow C, Murrell E, Holland JP, Kassenbrock A, Shannon W, Liang SH, Vasdev N, Stephenson NA (2020) Revisiting the radiosynthesis of [^{18}F] FPEB and preliminary PET imaging in a mouse model of Alzheimer's Disease. *Molecules* **25:** 982.

Vranesic I, Ofner S, Flor PJ, Bilbe G, Bouhelal R, Enz A, Desrayaud S, McAllister K, Kuhn R and Gasparini F (2014) AFQ056/mavoglurant, a novel clinically effective mGluR5 antagonist: identification, SAR and pharmacological characterization. *Bioorg Med Chem* **22:** 5790-5803.

Walles M, Wolf T, Jin Y, Ritzau M, Leuthold LA, Krauser J, Gschwind HP, Carcache D, Kittelmann M, Ocwieja M, Ufer M, Woessner R, Chakraborty A and Swart P (2013) Metabolism and Disposition of the Metabotropic Glutamate Receptor 5 Antagonist (mGluR5) Mavoglurant (AFQ056) in Healthy Subjects. *Drug Metab Dispos* **41:** 1626-1641.

JPET Fast Forward. Published on February 4, 2021 as DOI: 10.1124/jpet.120.000371
This article has not been copyedited and formatted. The final version may differ from this version.

Westerhout J, Danhof M, De Lange E (2011) Preclinical Prediction of Human Brain Target Site Concentrations: Considerations in Extrapolating to the Clinical Setting. *J Pharm Sci* **100:** 3577-3593.

Wong DF, Waterhouse R, Kuwabara H, Kim J, Brašić JR, Chamroonrat W, Stabins M, Holt DP, Dannals RF, Hamill TG and Mozley PD (2013)[a] ^{18}F-FPEB, a PET Radiopharmaceutical for Quantifying Metabotropic Glutamate 5 Receptors: A First-in-Human Study of Radiochemical Safety, Biokinetics, and Radiation Dosimetry *J Nucl Med* **54:** 388-96.

Wong DF, Kuwabara H, Poli SM, Gapasin L, Roberts J, Kitzmiller K and Duvauchelle T (2018)[b] An open label PET imaging study to evaluate the $mGlu_5$ receptor occupancy following ADX48621 (dipraglurant) administration. *XII International Symposium of Functional Neuroreceptor Mapping of the Living Brain, London, United Kingdom, 9 -12 July 2018* RF8.

Wyss MT, Ametamey SM, Treyer V, Bettio A, Blagoev M, Kessler LJ, Burger C, Weber B, Schmidt M, Gasparini F and Buck A (2007) A Quantitative evaluation of ^{11}C-ABP688 as PET ligand for the measurement of the metabotropic glutamate receptor subtype 5 using autoradiographic studies and a beta-scintillator. *Neuroimage* **35:** 1086-1092.

Xu Y and Li Z (2019) Imaging metabotropic glutamate receptor system: Application of positron emission tomography technology in drug development. *Medicinal Research Review* **39:** 1892-1922.

JPET Fast Forward. Published on February 4, 2021 as DOI: 10.1124/jpet.120.000371
This article has not been copyedited and formatted. The final version may differ from this version.

Footnotes

This work is fully funded by Sosei Heptares, Steinmetz Building, Granta Park, Great Abingdon, Cambridgeshire, CB21 6DG, UK.

JPET Fast Forward. Published on February 4, 2021 as DOI: 10.1124/jpet.120.000371
This article has not been copyedited and formatted. The final version may differ from this version.

Figure Legends

Figure 1. Relationship between exposure and receptor occupancy across multiple $mGlu_5$ NAM chemotypes. **A.** Exposure plotted as plasma C_{max} **B.** Exposure plotted as unbound plasma C_{max} divided by the affinity (K_i) of each ligand at the $mGlu_5$ receptor. The dotted line represents the theoretical curve-fit where 50 % occupancy is achieved when the unbound plasma = K_i. **C.** Exposure plotted as the unbound brain concentration divided by the affinity (K_i) of each ligand at the $mGlu_5$ receptor. The dotted line represents the theoretical curve-fit where 50 % occupancy is achieved when the unbound brain = Ki. Data was also fitted to a four-parameter sigmoidal dose-response curve (solid line).

Figure 2. Predicted vs measured $mGlu_5$ receptor occupancy of HTL0014242 across species. Comparison between the predicted (pred.) receptor occupancy (open icons) unbound plasma exposure versus the measured (meas.) receptor occupancy (filled icons) demonstrating that plasma levels underpredicts RO.

JPET Fast Forward. Published on February 4, 2021 as DOI: 10.1124/jpet.120.000371
This article has not been copyedited and formatted. The final version may differ from this version.

Tables

Table 1: $mGlu_5$ NAM inhibitor properties

Identifier		dipraglurant	mavoglurant	basimglurant	HTL0014242
Structure		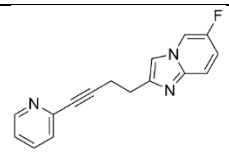	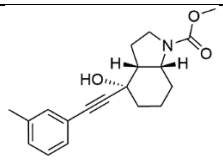	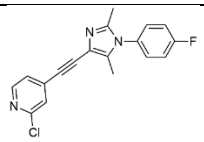	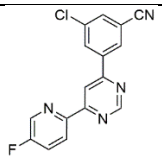
cLogP		2.58	3.16	4.71	3.04
$mGlu_5$ pK_i (mean ± SD)	**Human**	6.98 ± 0.24	7.95 ± 0.24	9.25 ± 0.40	9.30 ± 0.24
	Monkey	Not tested	Not tested	Not tested	8.88 (n=2) (8.71-9.05)
	Rat	7.21 (n=2) (7.20-7.22)	8.07 ± 0.16	8.93 (n=2) (8.81-9.06)	9.19 ± 0.11
	Mouse	7.13 ± 0.11	7.89 ± 0.42	Not tested	9.29 ± 0.18
Human plasma $T_{1/2}$ (h)		0.68-0.75[c]	12d	49-107[e]	N/A
Rat	**Fup**	0.037	0.15	0.021[b]	0.0028
	Fupr	0.13[a]	0.03[a]	N/A	0.0019
	Kp brain/ plasma	0.11	1.6	1.7[b]	1.9
	Kpuu	0.39	0.32	1.0[b]	1.3

[a] *Based on [CSF]/[total brain]*

[b] *Cited Fup and Kpuu assumed 1 based on cited good brain penetration (Lindermann et al., 2015)*

[c] *Tison et al., 2016*

JPET Fast Forward. Published on February 4, 2021 as DOI: 10.1124/jpet.120.000371
This article has not been copyedited and formatted. The final version may differ from this version.

[d] *Walles et al., 2013*

[e] *Cosson et al., 2018*

JPET Fast Forward. Published on February 4, 2021 as DOI: 10.1124/jpet.120.000371
This article has not been copyedited and formatted. The final version may differ from this version.

Table 2: Measured $mGlu_5$ receptor occupancy and associated exposure dosing for HTL0014242

Study	Oral Dose (mg/kg)	Ligand for RO	n RO	$mGlu_5$ RO (%) Mean ± SD	Satellite n For PK	Plasma (ng/mL) Mean ± SD	Total brain (ng/mL) Mean ± SD
Mouse *ex vivo*	2	[^{3}H]M-MPEP	5	42 ± 15	From RO animals	26 ± 9.03	50 ± 20.2
Rat *ex vivo*	1		5	69	From RO animals	78.6 ± 47.0	101 ± 37.7
	3		5	80		139 ± 22.8	162 ± 44.1
	10		5	91		652 ± 229	753 ± 219
Mouse *in vivo*	1		2	12 (0,24.7)	3	*9.3*[a]	*34*[a]
	3		2	73 (64, 83)	3	28 ± 9.38	102 ± 34.5
	10		2	88 (79,96)	3	160 ± 50.5	419 ± 166
	1[b]		3	24 ± 2.4	3	13 ± 11.7	100 ± 75.2
	3[b]		3	77 ± 13	3	120 ± 9.82	243 ± 39.6
	10[b]		3	95 ± 3.1	3	300 ± 42.2	577 ± 107
Rat PET study[c]	1	[^{18}F]FPEB	5	75	From RO animals	70.1 ± 30.7	225 ± 98.8
	10		5	85		207 ± 77.9	666 ± 251
Cyno PET study[c]	0.7		1	65	From RO animals	45	NA
	4		1	93		238	NA

[a] *Estimated assuming proportional from 3 mg/kg*

[b] *Administrated intraperitoneally*

[c] *Single RO computed as average of RO across each brain region*

JPET Fast Forward. Published on February 4, 2021 as DOI: 10.1124/jpet.120.000371
This article has not been copyedited and formatted. The final version may differ from this version.

Table 3: Mavoglurant, dipraglurant and basimglurant $mGlu_5$ RO and exposure

Compound/ Species	**Oral Dose Rat (mg/kg); Human (mg)**	**Ligand for RO**	**$mGlu_5$ RO (%) Mean ± SD**	**Plasma (ng/mL) Mean ± SD**	**Brain (ng/mL) Mean ± SD**
Mavoglurant/ rat[a]	3	[^{3}H]M-MPEP	45 ± 4	128 ± 64.2	204 ± 78.5
	10		73 ± 2	466 ± 178.4	641 ± 178.4
	30		83 ± 3	1002 ± 612.7	1505 ± 234.8
Basimglurant/ rat	N/A	[^{3}H]ABP688	50[b]	4.8[b]	*8.2*[c]
Basimglurant/ human	0.5	[^{11}C]RO511232[c]	25[d]	4.20[e]	*7.2*[f]
	1.5		53[d]	12.1[e]	*20.5*[f]
Dipraglurant/ human	100	[^{18}F]FPEB	27 ± 9.0[g]	1586[h]	*174*[i]
	200		44 ± 23[g]	3172[h]	*349*[i]
	300		54 ± 30[g]	4758[h]	*523*[i]

[a] *Values calculated from measured concentration (μM) presented in Bennett et al., 2014*

[b] *Quoted EC_{50} (Lindermann et al., 2015)*

[c] *Estimated based on Kp 1.7 (Lindermann et al., 2015)*

[d] *Quoted at Css (Quiroz et al., 2016) (PET study clinical trials.gov NCT01483469)*

[e] *Estimated from Css day 1 (Cosson et al., 2018) taking account of accumulation to Css*

[f] *Estimated at Css, assuming same brain partitioning as for rat*

[g] *Addex Therapeutics Initiating Report Life Science Capital 19 July 2016.*

[h] *From normalizing day 1 50 mg human plasma C_{max} reported (793 ng/ml) Tison 2016. Data consistent with reported plasma EC_{50} 2910±152 ng/ml (Wong et al., 2018[b])*

[i] *Brain estimated assuming same brain partitioning as measured in the rat (Kp 0.11)*

JPET Fast Forward. Published on February 4, 2021 as DOI: 10.1124/jpet.120.000371
This article has not been copyedited and formatted. The final version may differ from this version.

Table 4: Measured and predicted $mGlu_5$ RO for HTL0014242

Study	**Dose (mg/kg)**	**$mGlu_5$ RO Measured (%)**	**$mGlu_5$ RO predicted from [plasma]ub**	**$mGlu_5$ RO predicted from [brain]ub**	**Measured RO – Predicted RO from brain (%)[a]**
Mouse *ex vivo*	2	42 ± 15	16	19	23
Rat *ex vivo*	1	69	52	49	20
	3	80	66	61	19
	10	91	90	88	3.0
Mouse *in vivo*	1	12	6.4	14	-2.0
	3	73	17	33	41
	10	88	54	66	22
	1 – IP	24 ± 2.4	8.7	32	-8
	3 – IP	77 ± 13	47	54	23
	10 - IP	95 ± 3.1	69	73	22
Rat PET study	1	75	49	66	8
	10	85	74	87	-2
Cyno PET study	0.7	65	36	Not done	n/a
	4	93	75	Not done	n/a

[a] *Average RO underprediction ± standard deviation 14±14%*

JPET Fast Forward. Published on February 4, 2021 as DOI: 10.1124/jpet.120.000371
This article has not been copyedited and formatted. The final version may differ from this version.

Table 5: Measured and predicted $mGlu_5$ RO for mavoglurant, dipraglurant and basimglurant

Compound	Species	Dose Rat (mg/kg); Human (mg)	$mGlu_5$ RO Measured (%)	$mGlu_5$ RO predicted from [plasma]ub	$mGlu_5$ RO predicted from [brain]ub
Mavoglurant	Rat	3	45 ± 4	85	64
		10	73 ± 2	95	86
		30	83 ± 3	98	95
Basimglurant	Rat	N/A	50[a]	41	36
	Human	0.5	25	27	30
		1.5	53	51	56
Dipraglurant	Human	100	27 ± 9	66	43
		200	44 ± 23	80	60
		300	54 ± 30	85	69

[a] *Quoted EC_{50} (Lindermann et al., 2015)*

Figure 1

A

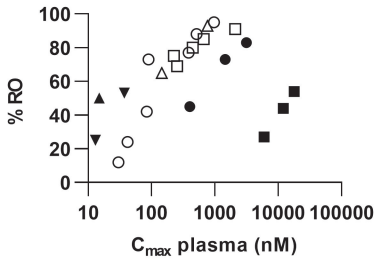
100
80
60
40
20
0
% RO
10
100
1000
10000
100000
C_{max} plasma (nM)

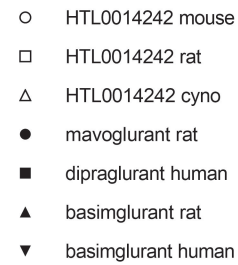
HTL0014242 mouse
HTL0014242 rat
HTL0014242 cyno
mavoglurant rat
dipraglurant human
basimglurant rat
basimglurant human

B

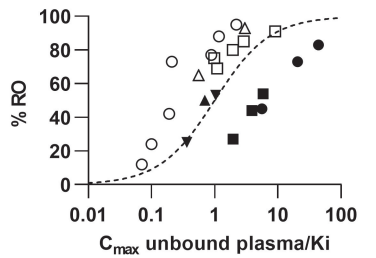
100
80
60
40
20
0
% RO
0.01
0.1
1
10
100
C_{max} unbound plasma/Ki

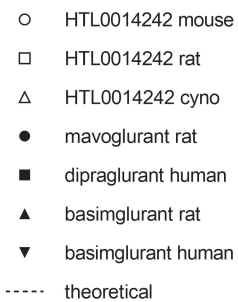
HTL0014242 mouse
HTL0014242 rat
HTL0014242 cyno
mavoglurant rat
dipraglurant human
basimglurant rat
basimglurant human
theoretical

C

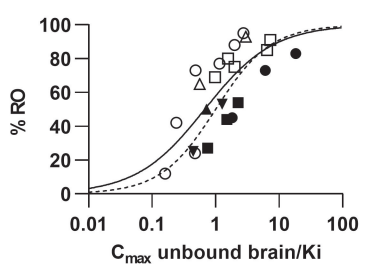
100
80
60
40
20
0
% RO
0.01
0.1
1
10
100
C_{max} unbound brain/Ki

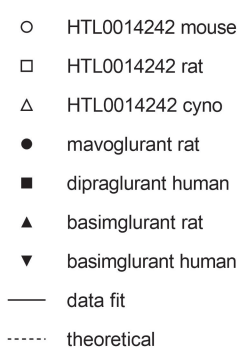
HTL0014242 mouse
HTL0014242 rat
HTL0014242 cyno
mavoglurant rat
dipraglurant human
basimglurant rat
basimglurant human
data fit
theoretical

Figure 2

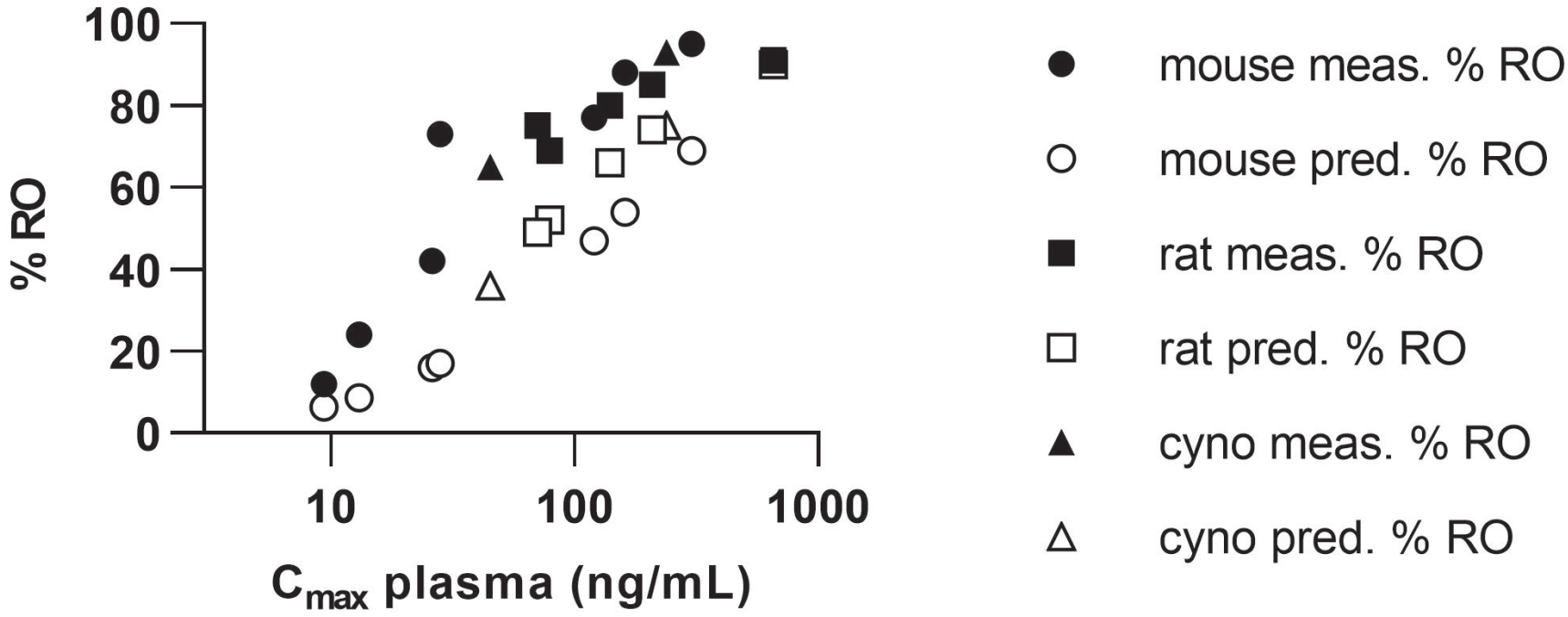
100
80
60
40
20
0
% RO
10
100
1000
C_{max} plasma (ng/mL)
mouse meas. % RO
mouse pred. % RO
rat meas. % RO
rat pred. % RO
cyno meas. % RO
cyno pred. % RO